

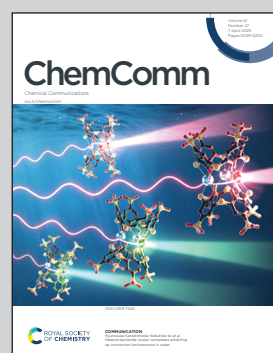
Showcasing research from Professor Habazaki's laboratory,  
Faculty of Engineering, Hokkaido University, Japan.

Thiosulfate species promoting hydrogen evolution reaction  
at the heterointerface of Ir clusters-loaded WS<sub>2</sub> nanosheets

Water molecule dissociation is promoted between positively  
charged thiosulfates and negatively charged Ir clusters at  
unique interfacial active sites in electrochemical hydrogen  
evolution reaction.

Image reproduced by permission of Sho Kitano from  
*Chem. Commun.*, 2025, **61**, 5114.

### As featured in:



See Sho Kitano, Hiroki Habazaki *et al.*,  
*Chem. Commun.*, 2025, **61**, 5114.



Cite this: *Chem. Commun.*, 2025, 61, 5114

Received 18th November 2024,  
Accepted 20th February 2025

DOI: 10.1039/d4cc06122e

rsc.li/chemcomm

## Thiosulfate species promoting hydrogen evolution reaction at the heterointerface of Ir clusters-loaded WS<sub>2</sub> nanosheets<sup>†</sup>

Sho Kitano,<sup>id \*a</sup> Reiko Tagusari,<sup>b</sup> Takeharu Sugiyama,<sup>c</sup> Yuta Nagasaka,<sup>b</sup> Naoto Wakabayashi,<sup>b</sup> Rioto Wada,<sup>b</sup> Tomoya Nagao,<sup>b</sup> Mana Iwai,<sup>a</sup> Koji Fushimi,<sup>a</sup> Yoshitaka Aoki<sup>id</sup><sup>a</sup> and Hiroki Habazaki<sup>id \*a</sup>

We synthesize Ir cluster-loaded monolayer WS<sub>2</sub> nanosheets for water electrolysis and fabricate unique functional heterointerfaces with thiosulfate species formed from sulfide ions of WS<sub>2</sub>. *In situ* XAFS measurements reveal that water dissociation is promoted between positively charged thiosulfates and negatively charged Ir clusters at the interfacial active sites for hydrogen evolution reaction.

Among various renewable energy technologies, water electrolysis is a promising method for producing clean hydrogen.<sup>1</sup> However, the widespread adoption of this technology has been hindered by the inefficiencies of the hydrogen evolution reaction (HER) and the oxygen evolution reaction (OER), and highly active catalysts are required to minimize the overpotential and improve the overall energy efficiency of the system.<sup>2</sup> Recently, it was discovered that compounds containing various typical elements such as metal sulfides, phosphides and nitrides showed high activity in HER or OER.<sup>3</sup> Although only constituent metal species have been considered to be active sites in HER or OER, it is gradually becoming clear that the adsorption of H or OH on neighboring sites, *i.e.*, typical elements, also plays important roles in the reaction. For example, in neutral and alkaline HERs where H<sub>2</sub>O is the substrate, it has been reported that the interaction of metal ions with O and sulfide ions with H on a metal sulfide electrocatalysts leads to the dissociation of H<sub>2</sub>O and the improvement of HER activities.<sup>4</sup> Therefore, in order to design highly efficient catalyst materials, it is essential to consider and analyze the properties of typical elements as well as metal species. Nevertheless, the properties of typical elements have not been sufficiently studied compared to metal species, and there are very few reports on *in situ*

measurements to clarify the behaviors and functionalities of typical elements in catalytic materials.<sup>5–7</sup> The construction of heterointerfaces by synthesizing composite materials has attracted attention to developing highly active catalytic materials.<sup>8–10</sup> Significant progress has been achieved in the development of highly active electrocatalysts by exploiting the unique properties of heterostructures, which are interfaces between different components that can produce synergistic effects not achievable with individual materials. Therefore, it is highly expected that the construction of heterointerfaces containing typical elements and the analysis of their behaviors will lead to the discovery of new breakthroughs. In a recent study, the authors synthesized composite catalysts consisting of monolayer metal hydroxide nanosheets and Au clusters, and outstanding OER performances were achieved at the heterointerfaces of the catalysts.<sup>11</sup> Since both monolayer nanosheets and metal clusters have a high surface area-to-volume ratio, the combination is an effective catalyst design that maximizes the material interfaces to utilize its functionalities. Metal sulfides such as WS<sub>2</sub> and MoS<sub>2</sub> are known as layered materials<sup>12</sup> and the monolayers of WS<sub>2</sub> and MoS<sub>2</sub> are preferred for construction of sulfur-containing heterointerfaces in composites of nanosheets and metal clusters and for development of new functionalities. In this study, to focus on the role of sulfur elements in the heterointerfaces, we synthesized a composite catalyst by combining WS<sub>2</sub> monolayer nanosheets and Ir clusters (Fig. 1(a) and Fig. S1, ESI<sup>†</sup>). Since Ir is active in both HER and OER under acid, neutral and alkaline conditions, heterointerfaces composed of Ir clusters are appropriate for investigating the effects of heterostructures on the reactions. Thiosulfate species are produced from S<sup>2–</sup> of WS<sub>2</sub> by natural oxidation through the combination of the Ir clusters and the WS<sub>2</sub> nanosheets. *In situ* XAFS measurements found that the dissociation of H<sub>2</sub>O molecules in the HER process is promoted by unique valence change of thiosulfate species. On the other hand, the thiosulfate species are simply oxidized and dissolved during the OER. This is the first report to demonstrate that sulfur oxoacid, thiosulfate, improves HER activity.

Monolayer WS<sub>2</sub> nanosheets were synthesized using the one-pot method as reported previously.<sup>13</sup> In the XRD patterns, the

<sup>a</sup> Division of Applied Chemistry, Faculty of Engineering, Hokkaido University, Sapporo, Hokkaido 060-8628, Japan

<sup>b</sup> Graduate School of Chemical Sciences and Engineering, Hokkaido University, Sapporo, Hokkaido 060-8628, Japan

<sup>c</sup> Research Center for Synchrotron Light Applications, Kyushu University, 6-1 Kasuga-koen, Kasuga, Fukuoka 816-8580, Japan

<sup>†</sup> Electronic supplementary information (ESI) available. See DOI: <https://doi.org/10.1039/d4cc06122e>



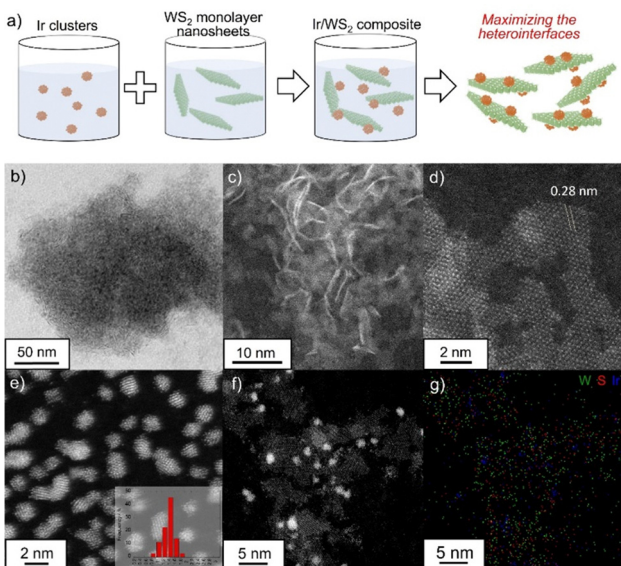


**Fig. 1** (a) Schematic illustration of fabrication of the Ir/WS<sub>2</sub> from monolayer WS<sub>2</sub> and Ir clusters. (b) Low-magnification TEM image of the monolayer WS<sub>2</sub> nanosheets. HAADF-STEM images of (c) and (d) the monolayer WS<sub>2</sub> nanosheets, (e) Ir clusters and (f) Ir/WS<sub>2</sub>. (g) STEM-EDX mapping of the Ir/WS<sub>2</sub>. (W: green, S: red, Ir: blue).

peak of the (002) reflection around 14° derived from the layer stacking, was not be observed for monolayer WS<sub>2</sub> nanosheets while the commercial WS<sub>2</sub> showed the strong and sharp peak (Fig. S2, ESI<sup>†</sup>).<sup>14</sup> The SEM-EDS results showed that W and S were uniformly distributed in the synthesized WS<sub>2</sub> (Fig. S3, ESI<sup>†</sup>), and the composition was W:S = 1:1.94, which is almost the ideal ratio. Transmission electron microscopy (TEM), high angle annular dark-field scanning transmission electron microscopy (HAADF-STEM) and atomic force microscopy (AFM) characterizations were conducted to investigate the morphology and structural characteristics of the synthesized WS<sub>2</sub> (Fig. 1(b), (c) and Fig. S4, ESI<sup>†</sup>). The TEM, HAADF-STEM and AFM images reveal that the nanosheets exhibit a uniform, two-dimensional morphology, with lateral sizes of several nanometers. The lattice fringes of the WS<sub>2</sub> nanosheets were clearly visible, with an interlayer spacing of approximately 0.28 nm, which corresponds to the (100) plane of hexagonal WS<sub>2</sub> (Fig. 1(d)).<sup>14</sup> The results clearly show the successful synthesis of monolayer WS<sub>2</sub> nanosheets. Colloidal Ir clusters were synthesized in a mixed solvent of ethylene glycol and water.<sup>15</sup> The STEM image (Fig. 1(e) and Fig. S5, ESI<sup>†</sup>) clearly showed that Ir clusters were uniformly dispersed without agglomeration and had an average size of approximately 1.4 nm. The STEM analysis also revealed that the Ir/WS<sub>2</sub> catalyst consisted of the monolayer WS<sub>2</sub> nanosheets and Ir clusters with uniform dispersion (Fig. 1(f), (g) and Fig. S6, ESI<sup>†</sup>). The lateral sizes of the WS<sub>2</sub> nanosheets in the Ir/WS<sub>2</sub> were smaller than those of the pristine WS<sub>2</sub> nanosheets, suggesting that WS<sub>2</sub> nanosheets were partially fragmented during the combination process due to the physically fragile nature of monolayer nanosheets. For comparison, the Ir cluster-loaded graphene (Ir/G) catalyst was also prepared, which showed a similar uniform dispersion of Ir clusters with an average particle size of 1.4 nm (Fig. S7, ESI<sup>†</sup>). The Ir/WS<sub>2</sub> and Ir/G showed similar electrochemical surface area (Fig. S8, ESI<sup>†</sup>).

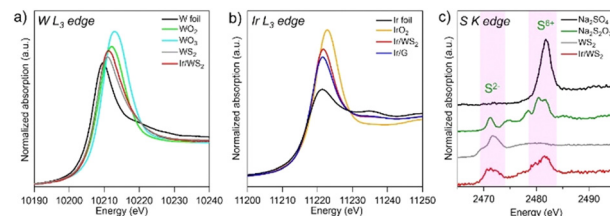


**Fig. 2** (a) W L<sub>3</sub>-edge, (b) Ir L<sub>3</sub>-edge and (c) S K-edge XANES spectra of the pristine WS<sub>2</sub>, Ir/WS<sub>2</sub>, Ir/G and reference compounds.

The SEM-EDX analysis indicated that the amount of Ir clusters loading was 73 wt% for the Ir/WS<sub>2</sub> and 63 wt% for the Ir/G, confirming that composite catalysts with similar Ir loading were successfully synthesized by using the combination method.

XAES and XPS measurements were conducted to investigate the oxidation states of component elements for the pristine WS<sub>2</sub>, Ir/WS<sub>2</sub> and Ir/G (Fig. 2 and Fig. S9, S10, ESI<sup>†</sup>). The pristine WS<sub>2</sub> showed the absorption edge attributable to W<sup>4+</sup> (10210.9 eV) in the W L<sub>3</sub>-edge XANES spectra, which was slightly higher than that of the laminated bulk WS<sub>2</sub> (10210.6 eV) (Fig. S10, ESI<sup>†</sup>). The absorption edge of the Ir/WS<sub>2</sub> (10211.2 eV) slightly shifted to the higher energy side than that of the pristine WS<sub>2</sub> (Fig. 2(a)), indicating that the W species in the Ir/WS<sub>2</sub> have more oxidative states compared to those of the pristine WS<sub>2</sub>. The WS<sub>2</sub> nanosheets were fragmented during the combination process with Ir clusters, resulting in partial oxidation of nanosheets. In the Ir L<sub>3</sub>-edge XANES spectra of the Ir/WS<sub>2</sub> and Ir/G (Fig. 2(b)), the absorption edges of the Ir/WS<sub>2</sub> and Ir/G were observed at 11221.8 eV and 11221.5 eV, respectively, which are between the Ir (Ir<sup>0</sup>) and IrO<sub>2</sub> (Ir<sup>4+</sup>). Since the average cluster size of 1.4 nm was very small, the spectra reflected the inner metallic states and the surface oxidative states of the Ir clusters. The absorption edge of the Ir/WS<sub>2</sub> catalyst was slightly higher than that of the Ir/G, indicating more oxidative states of the Ir clusters on the WS<sub>2</sub> than those on the graphene. In the S K-edge XANES spectrum of the pristine WS<sub>2</sub>, the peak at 2471.6 eV was observed, which is attributable to S<sup>2-</sup> species of typical sulfides (Fig. 2(c)).<sup>6</sup> On the other hand, the Ir/WS<sub>2</sub> showed two peaks at 2471 eV and 2482 eV in the spectrum, which are attributable to S<sup>2-</sup> and S<sup>6+</sup> species, respectively. The results suggest the formation of thiosulfate.<sup>16</sup> This is due to the oxidation of the S<sup>2-</sup> species during the combination process, leading to the formation of thiosulfate species with cationic S<sup>6+</sup> species on the entire surface of WS<sub>2</sub> (Fig. S11, ESI<sup>†</sup>).<sup>17</sup> Based on the measurements, electronic states of W and S in the Ir/WS<sub>2</sub> were partially changed to more oxidative states than those of the pristine WS<sub>2</sub> during the combination of Ir clusters and thiosulfate species formed in the Ir/WS<sub>2</sub>. In addition, EXAFS analysis suggested formation of heterointerfaces of Ir clusters and WS<sub>2</sub> (Fig. S12, ESI<sup>†</sup>).

The HER and OER activities of the synthesized catalysts were measured under acidic, neutral and alkaline conditions (Fig. 3, Fig. S13, S14 and Table S1, ESI<sup>†</sup>). The same measurements were also performed on Pt/C and IrO<sub>2</sub> samples for comparisons. Under alkaline and neutral conditions, the HER proceeds with H<sub>2</sub>O molecules as the substrate, whereas protons act as the substrate under acidic conditions, and the acidic HER proceeds without dissociation of the OH bond (acidic:  $2\text{H}^+ + 2\text{e}^- \rightarrow 2\text{H}_2$ , neutral,

alkaline:  $2\text{H}_2\text{O} + 2\text{e}^- \rightarrow \text{H}_2 + 2\text{OH}^-$ ).<sup>18</sup> In this study, all catalysts showed higher HER activities under the acidic condition than under the alkaline and neutral conditions. The Pt/C, a typical highly active catalyst for HER, exhibited high activities, while the Ir/G showed lower activities than the Pt/C under all conditions as reported previously.<sup>19</sup> While the WS<sub>2</sub> alone showed very low HER activities under all conditions, the Ir/WS<sub>2</sub> showed good HER activities, indicating that the Ir clusters act as the main active species in the Ir/WS<sub>2</sub>. Notably, the Ir/WS<sub>2</sub> showed lower HER activities than the Pt/C under the acidic condition, but showed comparable activities to the Pt/C under the alkaline and neutral conditions. Furthermore, although the Ir/WS<sub>2</sub> catalyst contains the same active Ir clusters as the Ir/G, the Ir/WS<sub>2</sub> showed similar activities to the Ir/G under the acidic condition, but showed much higher activities than the Ir/G under the alkaline and neutral conditions. This activity discrepancy clearly originated from the difference in the composite materials, *i.e.* WS<sub>2</sub> and graphene. The superior activities of Ir/WS<sub>2</sub> over Ir/G under the alkaline and neutral conditions suggest that the combination of Ir and WS<sub>2</sub> facilitates H<sub>2</sub>O dissociation. When comparing based on the current densities per Ir mass of the catalysts, the same activity order was observed in HER (Fig. S15, ESI†), and the similar conclusion was also obtained in the impedance measurements (Fig. S16, ESI†). In the OER, the WS<sub>2</sub> alone showed very low activities under all conditions, indicating that Ir clusters work as the active species in the Ir/WS<sub>2</sub> for OER (Fig. 3(d)–(f)). The Ir/WS<sub>2</sub> and Ir/G showed significantly higher activities than those of the IrO<sub>2</sub>, demonstrating that the Ir clusters can also act as a highly active OER catalyst.<sup>20</sup> The catalytic activities differed with pH, but the degree of difference in activities due to the difference in pH was smaller than the difference in activities in HER. In OER, H<sub>2</sub>O is the substrate under acidic and neutral conditions, and OH<sup>−</sup> is the substrate under alkaline conditions (acidic, neutral:  $2\text{H}_2\text{O} \rightarrow 4\text{H}^+ + \text{O}_2 + 4\text{e}^-$ , alkaline:  $4\text{OH}^- \rightarrow 2\text{H}_2\text{O} + \text{O}_2 + 4\text{e}^-$ ). Therefore, dissociation of the OH bond occurs in all conditions, leading to smaller activity differences with pH. The Ir/WS<sub>2</sub> showed higher OER activities than the Ir/G, but unlike HER, the difference in activities between the Ir/WS<sub>2</sub> and Ir/G was not large in any conditions. Therefore, it is believed that the functions of WS<sub>2</sub> and graphene as composite materials are similar in the OER process. When comparing the Ir/

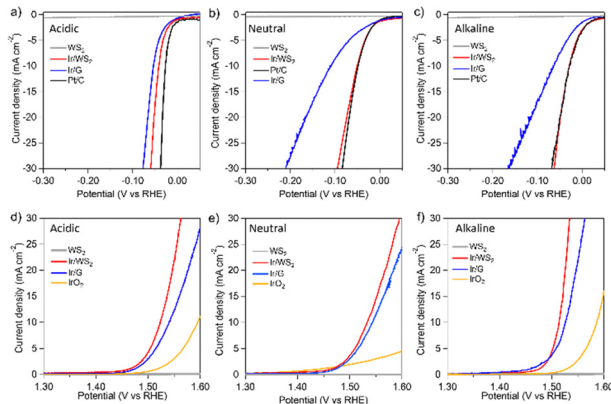


Fig. 3 IR-corrected polarization curves of the pristine WS<sub>2</sub>, Ir/WS<sub>2</sub>, Ir/G, Pt/C and IrO<sub>2</sub> for (a)–(c) HER and (d)–(f) OER in the aqueous solution of (a) and (d) 0.5 mol dm<sup>−3</sup> H<sub>2</sub>SO<sub>4</sub>, (b) and (e) 1 mol dm<sup>−3</sup> PBS, and (c) and (f) 1 mol dm<sup>−3</sup> KOH.

WS<sub>2</sub> and isolated Ir clusters without support materials, the similar results were observed (Fig. S13, ESI†).

*In situ* XAFS measurements were performed to investigate catalytic behaviors of the Ir/WS<sub>2</sub> under HER and OER conditions (Fig. 4). Under the initial OCP condition, the spectra were similar to the *ex situ* XAFS results. When a potential of −0.05 V vs. RHE was applied, the W L<sub>3</sub>-edge and Ir L<sub>3</sub>-edge XANES spectra shifted to lower energy sides. Under HER conditions where negative potentials are applied, electronic states of electrodes generally change to reductive.<sup>21</sup> Therefore, the W and Ir species in the Ir/WS<sub>2</sub> changed to reductive electronic states during HER. Under the OCP condition after the polarization, the W L<sub>3</sub>-edge and Ir L<sub>3</sub>-edge spectra returned to almost the same positions as the spectra under the initial OCP condition. On the other hand, the S K-edge spectra exhibited interesting behaviors. Under the initial OCP condition, peaks corresponding to S<sup>2−</sup> and S<sup>6+</sup> were observed at 2472 eV and 2482 eV, respectively, similar to the *ex situ* measurements (Fig. 4(e)). Under the polarization of −0.05 V vs. RHE, the intensity of the S<sup>2−</sup> peak decreased and that of the S<sup>6+</sup> peak increased, clearly indicating an oxidative change in the electronic states of the sulfur species despite the reductive condition of HER.<sup>17</sup> Notably, after returning to the OCP condition, the S K-edge spectrum returned to its initial states, suggesting reversible change in the electronic states of the sulfur species. This unique behavior suggests that the central S<sup>6+</sup> of the thiosulfate species interacts with the anionic O of H<sub>2</sub>O accompanied with charge attraction from thiosulfates to H<sub>2</sub>O at the Ir/WS<sub>2</sub> heterointerfaces. Since the W and Ir species were reduced under HER conditions, the cationic H of H<sub>2</sub>O is likely to interact preferentially with them.<sup>22</sup> The active site for HER is Ir, not W. Therefore, the dissociation of the OH bond is facilitated by the interaction between the central S<sup>6+</sup> of the thiosulfate species and the O of H<sub>2</sub>O, as well as the interaction between the Ir cluster and the H atom of H<sub>2</sub>O, resulting in excellent HER activities (Fig. S17(a), ESI†). The Ir/WS<sub>2</sub> exhibited higher HER activities than the Ir/G in alkaline and neutral media, while their activities were similar under

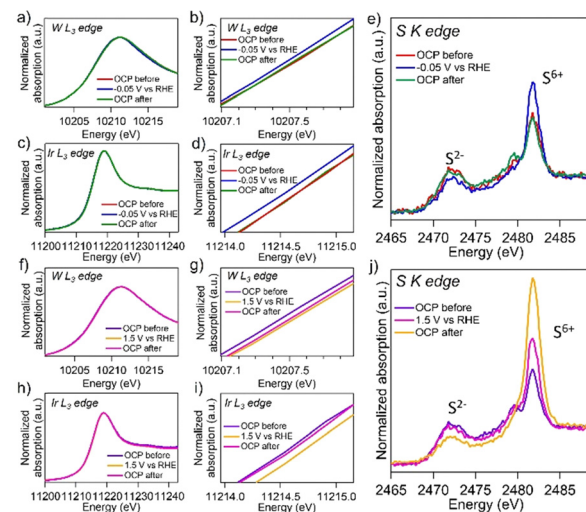


Fig. 4 *In situ* (a), (b), (f) and (g) W L<sub>3</sub>-edge, (c), (d), (h) and (i) Ir L<sub>3</sub>-edge, and (e) and (j) S K-edge XANES spectra of the Ir/WS<sub>2</sub> in the aqueous solution of 1 mol dm<sup>−3</sup> PBS. (b), (d), (g) and (i) are enlargements of (a), (c), (f) and (h), respectively.



acidic conditions. The HER activities of Ir/WS<sub>2</sub> in alkaline and neutral media were achieved by the thiosulfate-facilitated water dissociation at the heterointerface, which is the reason for the superior performances of the Ir/WS<sub>2</sub> those of the Ir/G. One possible explanation for the presence of S<sup>6+</sup> in the Ir/WS<sub>2</sub> is sulfate species rather than thiosulfate species. However, since the S<sup>2-</sup> peak decreased and the S<sup>6+</sup> peak increased reversibly, it is highly likely that thiosulfate species containing both S<sup>2-</sup> and S<sup>6+</sup> are present within the molecule. Furthermore, an Ir/WS<sub>2</sub> catalyst that does not contain thiosulfate species exhibited low HER activities, suggesting that thiosulfate species play an important role in enhancing HER activities (Fig. S18, ESI<sup>†</sup>). Catalytic behaviors of the Ir/WS<sub>2</sub> under OER conditions were also investigated. Under the polarization of 1.50 V vs. RHE, the W L<sub>3</sub>-edge and Ir L<sub>3</sub>-edge XANES spectra shifted to higher energy sides, indicating an oxidative change in electronic states of the W and Ir species (Fig. 4(f), (g), (h) and (i)). Under the OCP condition after the polarization, the Ir L<sub>3</sub>-edge XANES spectrum returned to its initial position, while the W L<sub>3</sub>-edge spectrum remained slightly shifted to higher energies, indicating partially irreversible oxidative alteration of WS<sub>2</sub>. The S K-edge spectra under the OER condition showed a decrease in the S<sup>2-</sup> peak intensity and an increase in the S<sup>6+</sup> peak intensity, suggesting an oxidative change in electronic states of sulfur species (Fig. 4(j)). However, when the potential was returned to OCP, the peak intensities of both did not return to their original levels. These results indicate that thiosulfates and the original S<sup>2-</sup> species were oxidized and the WS<sub>2</sub> nanosheets were degraded during the OER (Fig. S10(b), ESI<sup>†</sup>), as reported previously.<sup>23</sup> When the STEM observation and XRD measurement were performed on the Ir/WS<sub>2</sub> after HER and OER (Fig. S19 and S20, ESI<sup>†</sup>), the Ir/WS<sub>2</sub> after HER was almost the same as before the reaction, whereas the WS<sub>2</sub> nanosheets considerably disappeared and the Ir clusters were aggregated after OER. The Ir/WS<sub>2</sub> showed a similar polarization curve after 1000 cycles of CV measurement, indicating good durability of the Ir/WS<sub>2</sub> in HER (Fig. S21, ESI<sup>†</sup>). *In situ* XAFS measurements for the pristine WS<sub>2</sub>, which does not contain thiosulfate species, revealed that reversible change in the S K-edge spectra in HER was attributed to thiosulfate species in the Ir/WS<sub>2</sub> (Fig. S22, ESI<sup>†</sup>). This is the first study to find that the oxoacid of sulfur, thiosulfate, can improve HER activities. In summary, we synthesized the Ir/WS<sub>2</sub> electrocatalyst with maximized heterointerfaces and investigated the unique catalytic behaviors of thiosulfate species. The Ir/WS<sub>2</sub> showed excellent activities comparable to the Pt/C in HER under the neutral and alkaline conditions. *In situ* XAFS analysis revealed the unique functionality of thiosulfate species at the Ir/WS<sub>2</sub> heterointerface which promoted water dissociation during HER and that underwent oxidative dissolution during OER. Of the thiosulfate species generated on the surface, only those close to Ir clusters would contribute to HER activities. Recently, some studies found that several oxoacids such as SeO<sub>3</sub><sup>2-</sup> and phosphate enhanced HER activities based on the different mechanism from that of this study.<sup>24,25</sup> These findings in this study not only emphasize functionalities of typical elements at the heterointerfaces for electrocatalytic water splitting, but also

suggest a broader application potential for oxoacid-enhanced activities in electrocatalysis fields.

## Data availability

All data can be found in the main article or the ESI.<sup>†</sup>

## Conflicts of interest

There are no conflicts to declare.

## Notes and references

1. S. Chu and A. Majumdar, *Nature*, 2012, **488**, 294.
2. H. Wu, Q. X. Huang, Y. Y. Shi, J. W. Chang and S. Y. Lu, *Nano Res.*, 2023, **16**, 9142.
3. M. I. Jamesh, D. Q. Hu, J. Wang, F. Naz, J. P. Feng, L. Yu, Z. Cai, J. C. Colmenares, D. J. Lee, P. K. Chu and H. Y. Hsu, *J. Mater. Chem. A*, 2024, **12**, 11771.
4. J. Staszak-Jirkovsky, C. D. Malliakas, P. P. Lopes, N. Danilovic, S. S. Kota, K. C. Chang, B. Genorio, D. Strmcnik, V. R. Stamenkovic, M. G. Kanatzidis and N. M. Markovic, *Nat. Mater.*, 2016, **15**, 197.
5. W. Zhang, X. K. Liu, T. Liu, T. Chen, X. Y. Shen, T. Ding, L. L. Cao, L. Wang, Q. Q. Luo and T. Yao, *J. Phys. Chem. C*, 2021, **125**, 6229.
6. M. Q. Liu, J. A. Wang, W. Klysubun, G. G. Wang, S. Sattayaporn, F. Li, Y. W. Cai, F. C. Zhang, J. Yu and Y. Yang, *Nat. Commun.*, 2021, **12**, 5260.
7. B. Lassalle-Kaiser, D. Merki, H. Vrubel, S. Gul, V. K. Yachandra, X. L. Hu and J. Yano, *J. Am. Chem. Soc.*, 2015, **137**, 314.
8. X. Wu, Q. Yan, H. Wang, D. Y. Wu, H. Zhou, H. Li, S. Yang, T. Y. Ma and H. Zhang, *Adv. Funct. Mater.*, 2024, **34**, 2404535.
9. S. Kitano, H. Motohashi, M. Iwai, K. Fushimi, Y. Aoki and H. Habazaki, *Appl. Surf. Sci.*, 2024, **670**, 160552.
10. Q. Shao, P. T. Wang and X. Q. Huang, *Adv. Funct. Mater.*, 2019, **29**, 1806419.
11. S. Kitano, T. G. Noguchi, M. Nishihara, K. Kamitani, T. Sugiyama, S. Yoshioka, T. Miwa, K. Yoshizawa, A. Staykov and M. Yamauchi, *Adv. Mater.*, 2022, **34**, 2110552.
12. X. Wu, H. B. Zhang, J. Zhang and X. W. Lou, *Adv. Mater.*, 2021, **33**, 2008376.
13. C. Altavilla, M. Sarno and P. Ciambelli, *Chem. Mater.*, 2011, **23**, 3879.
14. Z. Y. Ni, H. Wen, S. Q. Zhang, R. Guo, N. Su, X. W. Liu and C. M. Liu, *ChemCatChem*, 2020, **12**, 4962.
15. J. F. Cheng, J. Yang, S. Kitano, G. Juhasz, M. Higashi, M. Sadakiyo, K. Kato, S. Yoshioka, T. Sugiyama, M. Yamauchi and N. Nakashima, *ACS Catal.*, 2019, **9**, 6974.
16. M. E. Fleet, X. Y. Liu, S. L. Harmer and P. L. King, *Can. Mineral.*, 2005, **43**, 1605.
17. D. W. Wang, Q. Li, C. Han, Z. C. Xing and X. R. Yang, *ACS Cent. Sci.*, 2018, **4**, 112.
18. M. Durovic, J. Hnáť and K. Bouzek, *J. Power Sources*, 2021, **493**, 229708.
19. Z. W. Seh, J. Kibsgaard, C. F. Dickens, I. B. Chorkendorff, J. K. Norskov and T. F. Jaramillo, *Science*, 2017, **355**, eaad4998.
20. L. W. Chen and H. W. Liang, *Catal. Sci. Technol.*, 2021, **11**, 4673.
21. Y. P. Zhu, T. R. Kuo, Y. H. Li, M. Y. Qi, G. Chen, J. L. Wang, Y. J. Xu and H. M. Chen, *Energy Environ. Sci.*, 2021, **14**, 1928.
22. C. Cai, K. Liu, L. Zhang, F. B. Li, Y. Tan, P. C. Li, Y. Q. Wang, M. Y. Wang, Z. X. Feng, D. M. Meira, W. Q. Qu, A. Stefancu, W. Z. Li, H. M. Li, J. W. Fu, H. Wang, D. S. Zhang, E. Cortés and M. Liu, *Angew. Chem., Int. Ed.*, 2023, **62**, e202300873.
23. K. Kawashima, R. A. Márquez, L. A. Smith, R. R. Vaidyula, O. A. Carrasco-Jaim, Z. Q. Wang, Y. J. Son, C. L. Cao and C. B. Mullins, *Chem. Rev.*, 2023, **123**, 12795.
24. L. H. Zhou, C. M. Yang, W. C. Zhu, R. Li, X. X. Pang, Y. Z. Zhen, C. T. Wang, L. J. Gao, F. Fu, Z. W. Gao and Y. C. Liang, *Adv. Energy Mater.*, 2022, **12**, 2202367.
25. M. N. Jackson, O. Jung, H. C. Lamotte and Y. Surendranath, *ACS Catal.*, 2019, **9**, 3737.

